Satellite ASTER Geoscience Product Notes
Northern Territory

This document provides descriptions of the publicly available, ASTER geoscience products (Version 1) for the Northern Territory (NT; **Table 2** - page 16), including: (i) how the products were generated; (ii) accuracy; and (iii) examples of how they can be used for different geological applications. There are fourteen geoscience products based on ASTER's nine visible, near-infrared (VNIR) and shortwave infrared (SWIR) "reflected" bands as well as two products from ASTER's five thermal infrared (TIR) bands (**Table 3** - page 22). There are another three TIR products still being validated prior to their release (**Table 4** - page 22). Note that the TIR products do not have the same level of calibration/validation as the VNIR-SWIR bands. The NT ASTER geoscience maps can be obtained from: (i) the NT webserver (Geophysical Image Web Server) - http://geoscience.nt.gov.au/giws/; (ii) the Northern Territory Geological Survey (NTGS) who can provide all the digital products (~500 Gigabytes) on an external drive; or (iii) CSIRO's web-portals (http://c3dmm.csiro.au; http://portal.auscope.org/portal/gmap.html) where only the final GIS-compatible products (e.g. geoTIFs) are available.

ASTER Geoscience Product Version:	1
Document version date:	3rd April 2012
Prepared by:	Thomas Cudahy

WA Centre of Excellence for 3D Mineral Mapping (C3DMM),
Minerals Down Under Flagship (MDU)
CSIRO Earth Science and Resource Engineering
Australian Resources Research Centre (ARRC)
26 Dick Perry Avenue, Kensington, Western Australia, 6151

Introduction

The 2020 vision for the Western Australian (WA) Centre of Excellence for 3D Mineral Mapping (C3DMM), which is part of CSIRO's Minerals Down Under (MDU) Flagship (http://www.csiro.au/org/MineralsDownUnderFlagship.html), is the generation of a three dimensional (3D) map of mineralogy (including species, abundance, chemistry and crystallinity) of the Australian continent based on a new generation of drill-core (http://nvcl.csiro.au), field, airborne and satellite sensing optical systems. This mineral information has the potential to benefit not just the Australian minerals community but also the energy, agriculture, water management and environmental sectors, who all face the challenges of a changing climate and dwindling resources.

The overall objective of CSIRO's Australian ASTER initiative is to provide National, public, web-accessible, GIS-compatible ASTER geoscience maps (chiefly, mineral groups) of Australia, suitable for mapping from the continental-scale down to 1:50,000 prospect-scale. This provides an opportunity for establishing related (National) standards, including: (1) geoscience product nomenclature; (2) processing methods; (3) accuracy assessments; and (4) traceable documentation. Fundamental to this initiative is the development and publication of processing methods and quality control (QC) measures that are universally applicable and easy to implement, which this document is a part.

The first and to date only geoscience-tuned[1] Earth observation (EO) system that has acquired complete coverage of the Australian continent is the Japanese ASTER (Advanced Spaceborne Thermal Emission and Reflectance Radiometer - http://asterweb.jpl.nasa.gov) system. ASTER was launched in December 1999 onboard the USA's Terra satellite (http://terra.nasa.gov, NASA's Earth Observing System, 2011). This multispectral satellite system has 14 spectral bands spanning: the visible and near-infrared (VNIR - 500-1000 nm – 3 bands @ 15 m pixel resolution); shortwave-infrared (SWIR – 1000-2500 nm range – 6 bands @ 30 m pixel resolution); and thermal infrared (TIR 8000-12000 nm - 90 m pixel resolution) atmospheric windows in a polar-orbiting, 60 km swath (Abrams *et al.,* 2002). However, the ASTER spectral bands do not have sufficient spectral resolution to accurately map the often small diagnostic absorption features of specific mineral species, which can be measured using "hyperspectral" (hundreds of spectral bands) systems[2] (http://speclab.cr.usgs.gov/hyperspectral.html). Thus ASTER data can only be used to map mineral groups, such as the di-octahedral "Al-OH" group comprising the mineral sub-groups (and their minerals species) like kaolins (e.g. kaolinite, dickite, halloysite), white micas (e.g. illite, muscovite, paragonite) and smectites (e.g. montmorillonite and beidellite).

The reduction of the ASTER Level 0 "instrument" data to Level 2 "reflectance" products by ERSDAC's Ground Data Segment (GDS - www.gds.aster.ersdac.or.jp) involves the correction for instrument, illumination, atmospheric and geometric effects. This methodology is described

---

[1] High spatial (<50m pixel) sensor designed to capture diagnostic mineralogical absorptions.
[2] A suite of civilian satellite hyperspectral imaging systems will be coming on stream for global geoscience mapping from 2015 (www.isiwg.org). Airborne hyperspectral systems currently exist, e.g. the airborne HyMap from Australia (www.hyvista.com).

in the ASTER Science Team's "Algorithm Theoretical Basis Documents" (www.science.aster.ersdac.or.jp/en/documnts/atbd.html). Though also formerly available from the USGS data portal in Sioux Falls, ASTER data for non-US-science users is now only accessible through the Japanese GDS.

There have been various workers exploring the use of ASTER imagery for geoscience mapping applications (e.g. Rowan *et al.,* 2003; Rowan and Mars, 2003; Hewson *et al.,* 2005; Ninomiya *et al.*, 2005; Cudahy et al., 2005, 2007; Hewson and Cudahy, 2010). However, there are currently no global standards for ASTER "geoscience products", i.e. no standard "mineral" products, though there is a global ASTER digital elevation product (GDEM - http://www.gdem.aster.ersdac.or.jp). Higher level mineral information products are of value to geoscientists as demonstrated by the fact that over 60,000 GIS compatible mineral maps from the Geological Survey of Queensland's (GSQ) North Queensland hyperspectral surveys were downloaded over the web (http://c3dmm.csiro.au). In contrast, less than a handful of radiance or reflectance products were requested by users in similar public airborne hyperspectral data releases by government geosurveys across Australia. This is because of the complexity of the image processing where users must rely on specialists to generate their geoscience information requirements. This has resulted in a plethora of non-standard methods and products being generated of differing quality, which has potentially limited the global geoscience value/impact of ASTER.

To help tackle this problem of a lack of "National standards", Geoscience Australia (GA) developed an ASTER image processing methodology based on published materials (http://www.ga.gov.au/image_cache/GA8238.pdf). These were then applied to a number of geologic regions across Australia (Oliver and van der Wielen, 2005). This was a major step forward though the user community found that the derived geoscience information products suffered problems with accuracy, related to insufficient removal of complicating effects, such as SWIR cross-talk (Iwasaki and Tonooka, 2005; Hewson and Cudahy, 2010) and the lack of masks to remove those pixels/areas either: (i) complicated by other factors (e.g. green vegetation, water, dark surfaces, clouds); or (ii) below the detection limits of the desired parameter (Cudahy *et al.*, 2008).

CSIRO's Australian ASTER Geoscience Map initiative with the government geosurveys across Australia began in the 1990's though it was not until late 2009 that this opportunity became achievable when access to the complete archive of ASTER imagery over Australia was secured (http://c3dmm.csiro.au/ASTER%20Map%20of%20Australia%20EOI%20flyer.pdf). This National initiative is now supported by State, Territory and Federal government geoscience agencies across Australia as well as the ASTER Science Team (http://www.science.aster.ersdac.or.jp/en/science_info/index.html), ERSDAC, NASA-JPL, United States Geological Survey and Auscope Grid (http://www.auscope.org.au/site/grid.php).

One of the keys to success for CSIRO's ASTER initiative has been access to an extensive archive of satellite Hyperion hyperspectral imagery (~2700 scenes across Australia - Figure 1) which has been critical for reduction and validation of the processed ASTER data. Global public access to ASTER and Hyperion imagery thus opens up the opportunity for extending this ASTER geoscience mapping around the world. However, this is only suitable for ASTER's nine VNIR-SWIR bands. There is currently no global, independent TIR data set suitable for

reducing/validating ASTER's five TIR bands though there is a publicly available, emissivity product (http://eospso.gsfc.nasa.gov/eos_homepage/for_scientists/atbd/docs/ASTER/atbd-ast-03.pdf). Hulley and Hook (2009) have also developed a new "temperature-emissivity separation" (or TES) algorithm which they have used to generate a mosaic of North America (http://hyspiri.jpl.nasa.gov/downloads/public/2010_Workshop/day3/day3_17_Hulley_HyspIRI_2010.pdf) and are now extending to other parts of the Earth (Hook, *pers. comm.*, 2011).
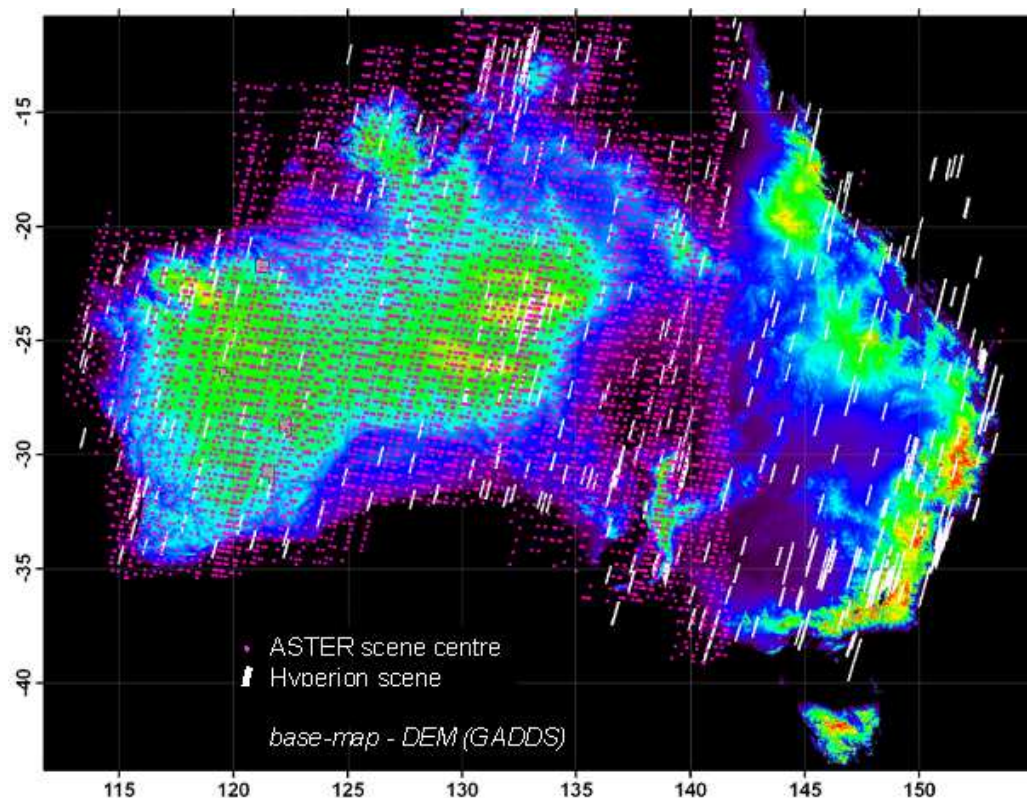

Figure 1: Map of Australia showing the location of the ASTER scene centres (pink dots) supplied by the USGS (up until June 2011 – the rest of Australia has since been delivered), together with locations of the satellite Hyperion and airborne HyMap surveys used in the reduction and validation process. Base colour image is a digital elevation model access from GA's data portal (www.geoscience.gov.au/bin/ mapserv36?map=/public/http/ www/geoportal/gadds/gadds. map&mode=browse).

This Northern Territory ASTER Geoscience Map is the third State/Territory release to date and follows on from earlier development and testing projects including: (1) Kalgoorlie (2 scenes -Cudahy et al, 2005; (2) the Gawler-Curnamona Blocks in South Australia (~20 scenes – Hewson et al, 2005); (3) the Mount Isa Block (140 scenes – Cudahy et al, 2008); WA ASTER maps (~1700 scenes); and (4) SA ASTER map (~800 scenes), all of which have been supported by Geoscience Australia. The complete Australian Geoscience Map is to be publicly released at the 34th International Geological Convention in Brisbane, in August 2012 (www.34igc.org). These maps will also be Version 1, though it is

acknowledged that there remain significant opportunities to improve on the accuracy (seamlessness) of the Version 1 methods/products in later updates, including: (1) green vegetation unmixing/removal; (2) instrument line-striping removal; and (3) integration with the National Vortual Core Library drill-core spectral database.

Processing methodology for the ASTER's VNIR-SWIR bands

The following is a summary of the background and methodology involved in processing the multi-scene ASTER imagery.   Detailed accounts will be provided in related publications.

Physical model

The ASTER processing methodology for the nine VNIR-SWIR bands follows that developed by Hewson et al (2005), Cudahy et al (2008) and Hewson and Cudahy (2010).   The model is:

$$L_{\lambda j} = (\frac{S_{\lambda,\Theta}}{\pi}.A_{\lambda}^{t}.R_{\lambda j}B_{j,\Theta}.T_{j} + A_{\lambda}^{s}).I_{\lambda}^{m} + I_{\lambda}^{a} \qquad\qquad (1)$$

where:
  L is the ASTER L1B radiance at sensor (W/m^2/sr);
  λ is wavelength (μm);
  j is pixel (m^2);
  Θ is angle (sr);
  S is solar irradiance (W/m^2/sr);
  A^t is atmospheric transmission;
  A^s is atmospheric scattering;
  R is surface bi-directional reflectance (includes both albedo and the desired "spectral shape" information);
  B is surface bi-directional reflectance distribution function (sr^{-1});
  T is topographic slope;
  I^a is an additive instrument affect; and
  I^m is a multiplicative (gain) instrument affect.

Note that the terms *A, R, B, T* and *I* are all dimensionless.

Assumptions with this model (1) include:
- No pixel-dependent A^t and A^s effects; and
- *B* is wavelength-independent and multiplicative for geological materials.

It is also assumed that the instrument gain, I^m, is accurately measured and corrected in the "as-received" ASTER L1B data such that I^m can be removed from Equation 1 and the additive terms, I^a and A^s, can be grouped together as follows:

$$L_{\lambda j} = (\frac{S_{\lambda,\Theta}}{\pi}.A_\lambda^t.R_{\lambda j}B_{j,\Theta}.T_j) + (A_\lambda^s + I_\lambda^a) \qquad (2)$$

Thus estimation and correction (removal) of the two additive terms[3], A^s and I^a, allows the use of normalisation procedures (e.g. ratio of two bands from the same pixel) to cancel all terms on the right-hand side of Equation 2 except for the desired *R*, albeit with its "albedo" ("average" pixel reflectance, labelled *Z*) also removed, leaving the desired, compositionally-diagnostic variation between spectral bands, called, *R**. That is:

$$\frac{L_{\lambda j}}{L_{(\lambda+x) j}} = \frac{\frac{S_{\lambda,\Theta}}{\pi}.A_\lambda^t.(Z_j.R_{(\lambda+x),j}^*).B_{j,\Theta}.T_j}{\frac{S_{(\lambda+x),\Theta}}{\pi}.A_{(\lambda+x)}^t.(Z_j.R_{(\lambda+x),j}^*).B_{j,\Theta}.T_j} \qquad (3)$$

$$= \frac{C_\lambda.R_{\lambda j}^*}{D_{(\lambda+x)}.R_{(\lambda+x) j}^*} \qquad (4)$$

where:

       Z is the pixel "albedo" (average surface reflectance)
       R* is the albedo-removed spectral signature
       C and D are constants; and
       x is an integer

---

[3] The importance of accurately estimating and correcting the additive component as part of the process for extracting temporally stable (independent of illumination conditions), accurate geoscience information products is described by Hewson and Cudahy (2010).

Note that $R*$ typically represents only a fraction of the original signal (can be <5%).   Thus instrument noise, both random (white or "shot" noise) and systematic (e.g. striping), is commonly observed in the final geoscience products.   For example, column striping becomes evident in the VNIR-SWIR bands, which is related to small but uncorrected mis-calibrations between detector elements in the sensor push-broom area detector array. In contrast, the TIR products yield line-striping which is a function of its whiskbroom imaging design. The important point regards QC is that successful removal of all of the obscuring effects shown in Equations 1-4 will often yield noisy geoscience products. Observing this noise is an indication of successful pre-processing. These types of instrument noise can in theory be removed though the desired geological information should nonetheless be evident.

VNIR SWIR image processing methodology

From the above Section, it is important to accurately estimate and remove the combined additive terms, A^s and I^a, in Equation 2 so that Equation 4 can then be used to extract the spectrally diagnostic compositional information. Inadequate correction of these additive components will yield error, especially for "darker" pixels.   Evidence for mis-calibration includes:

- Deeply shaded areas, such as on steep hillsides, showing solid "colour" where instead only random noise should be apparent;

- The spectral colour on the shaded sides of hills being different from the sunlit sides of the same hills (assuming the same surface composition); and

- There is correlation between the normalised product and the reflectance data, which can be assessed using scattergrams.

Three other steps are intrinsic to the Version 1 processing methodology, namely:

1. Masking to remove complicating effects, including dense green vegetation, cloud, deep shadows and water;

2. Masking/thresh-holding to include only those pixels that comprise the "diagnostic" spectral signatures. That is, final geoscience products images may show large areas of "null" data; and

3. Any between-scene variations related for example to changes in atmospheric transmission, aerosol scattering and/or residual SWIR cross-talk effects[4], can be estimated statistically allowing for all scenes to then be adjusted (gains and offsets) to a global scene response.

---

[4] After standard ERSDAC SWIR crosstalk correction (Iwasaki and Tonooka, 2005).

The following is a summary of the ASTER image processing procedure. Details will be provided in related publications currently in preparation.

1. Acquisition of the required ASTER L1B radiance@sensor data with SWIR cross-talk correction applied (www.gds.aster.ersdac.or.jp). Note that ASTER L2 "surface radiance" or "surface reflectance" can also be used;

2. SWIR Cross-talk correction (ERSDAC GDS software);

3. Geometric correction;

4. Converting the three 15 m VNIR bands to 30 m pixel resolution;

5. Generating a single nine band VNIR-SWIR image file (L1B) for each ASTER scene;

6. Solar irradiance correction;

7. Masking clouds and green vegetation;

8. Generation of ERMapper headers;

9. Calculation of statistics for masked-image overlaps and global scene response;

10. Scene ordering (best scenes up front in the mosaic);

11. Application of gains and offsets to cross-calibrate all images to a global response;

12. Reduction to "surface" reflectance using independent validation data (e.g. satellite Hyperion data). This requires selecting overlapping "regions of interest" (ROI) and calculating statistics to generate regression coefficients (gains and offsets). Alternatively, if independent EO data are not available then an estimate of the additive component (Equations 1 and 2) can be measured using a "dark-pixel" approach.   The "dark pixel" can be estimated using: (1) deep water (very effective for SWIR bands away from sun glint angle); or (2) extrapolation to the dark-point using at least different materials illuminated under a range of different topographic conditions;

13. Application of the correction data (offset +/- gain for each band per scene/mosaic);

14. Geoscience information extraction: Application of "normalisation" scripts (see Tables 1 and 2 for product details);

15. QC of normalised products using methods such as:

    o   Images are "flat" with both sides of topographic relief showing the same colour information. That is, the surface composition is not dependent on topographic shading;

    o   Appearance of spatially-apparent "random" pixel behaviour in areas of deep shade or water (in SWIR);

    o   No correlation between normalised products and non-normalised spectral bands; and

    o   Relationships to published geology and associated ASTER products;

16. Application of product masks/thresholds to generate the final suite of geoscience products. This includes the "composite mask" which comprises estimates for albedo, water and cloud (details provided in Table 1) as well as green vegetation cover (different levels depending on the geoscience product);

17. Carving the Territory -wide mosaic into smaller, web-accessible 1:1,000,000 map sheets (Figure 2); and

18. Contrast stretching and colour rendering to generate GIS-compatible products (e.g. geoTIF).
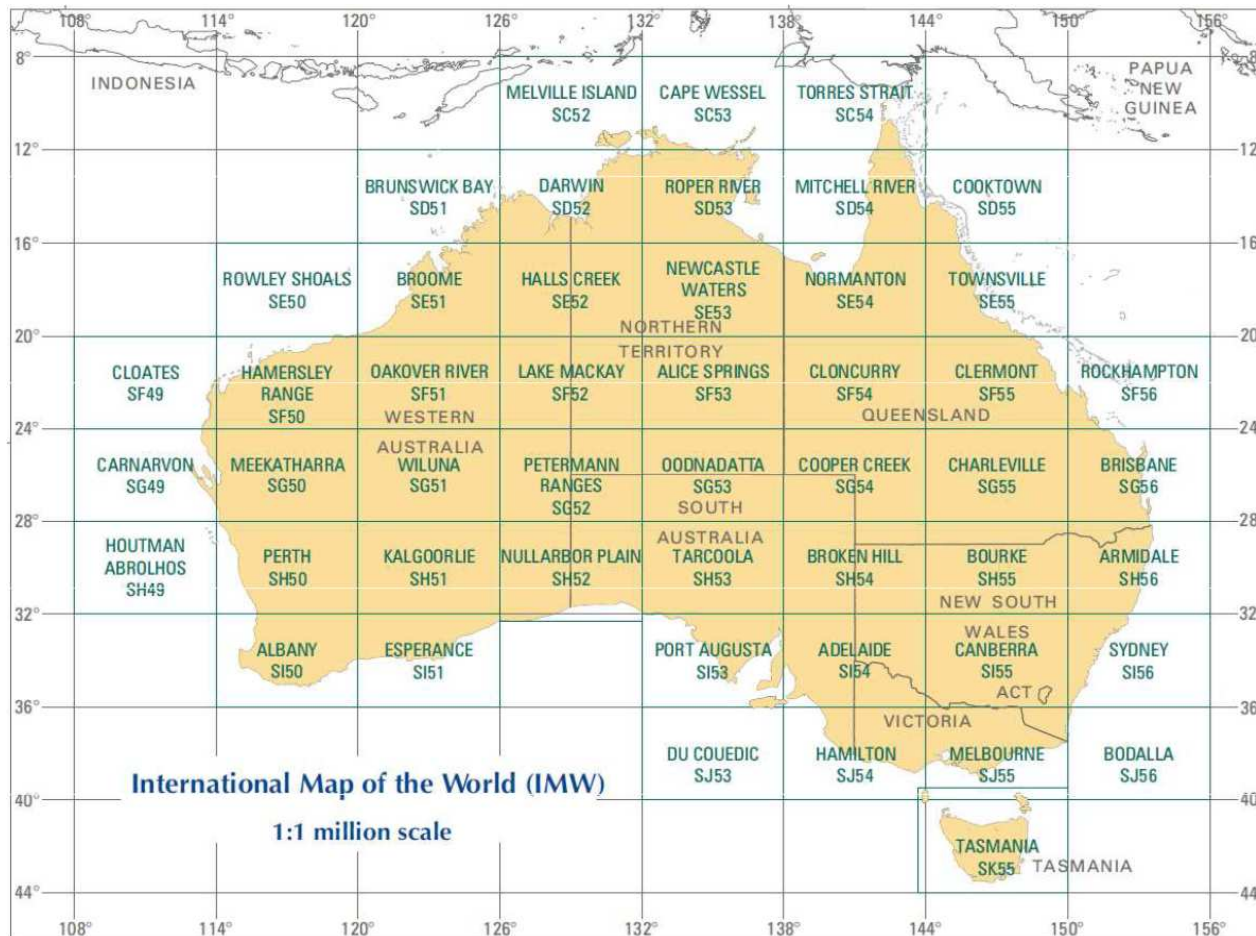

Figure 2: Map of Australia showing the approximate boundaries of the 1:1,000,000 map-sheet series (from www.ga.gov.au).

To expedite the seamless joining of the ASTER geoscience maps across the WA-SA-NT borders, the following methodology was applied:

- The gains and offsets generated for the WA-SA Hyperion-ASTER calibration were applied to the NT ASTER mosaic;
- The accuracy of the these corrections was tested using a selection of eight Hyperion scenes across NT, including the most western, northern, southern and eastern cloud free images, which were first processed to reflectance and then convolved to ASTER band configuration. Coincident ROI's from both the ASTER and Hyperion imagery were then collected (~140) from vegetation-free, bright, dark and mid-tone spatial-clusters of "homogenous" pixels; and
- The Hyperion images were then processed using the same band ratios as the WA-corrected SA ASTER mosaic to see if similar mineralogical/geological information was apparent.

The results of this validation process for bands 1, 4 and 9 (Figures 3a, 3b and 3c, respectively) show strong linear correlations between the coincident Hyperion reflectance and ASTER radiance/reflectance ROI data. Furthermore, the gains/offsets generated from the WA calibration procedure and applied to the NT ASTER mosaic result in the NT data more closely tracking the ideal y=x line. This indicates that the use of the WA regression data has improved the NT ASTER calibration.
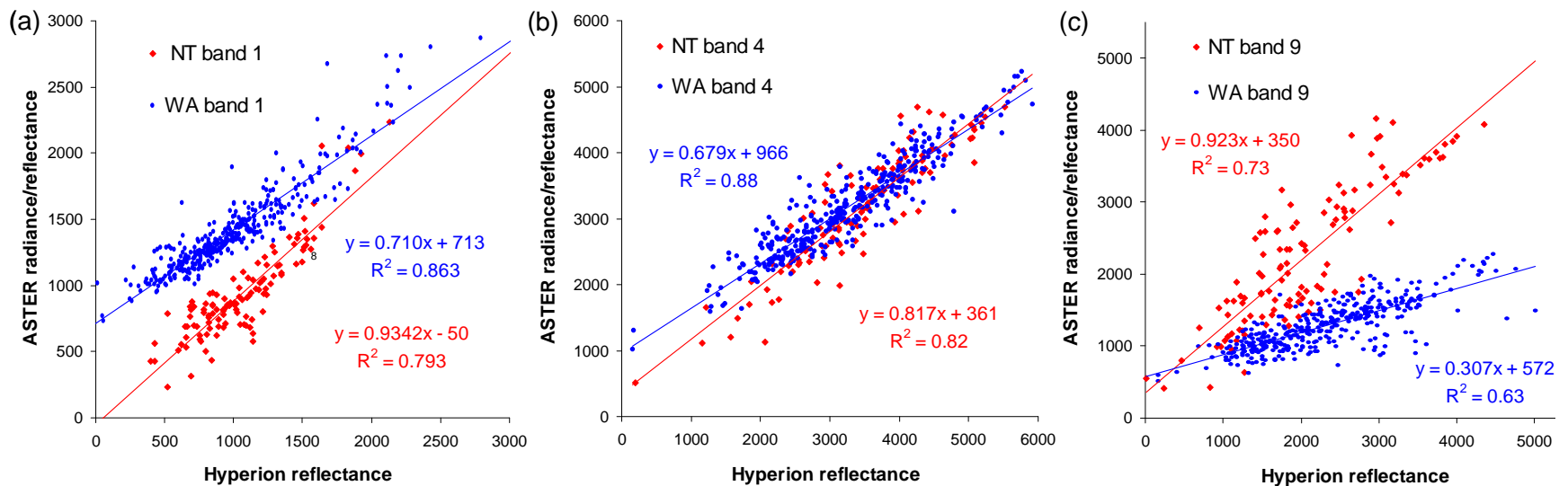

Figure 3. Scatter-grams of bands 1 (a), 5 (b) and 9 (c) of the Hyperion versus ASTER radiance/reflectance data for Western Australian (blue dots - without coefficients applied) and the Northern Territory (red dots - with coefficients applied) coincident regions of interest.

Table 1 plots the NT Hyperion versus ASTER mosaic ROI regression results for bands 1-9. This shows that the regression offsets generated using a linear fit typically represents less than 15% of the average apparent reflectance of each band. Although this is still not close to ideal of a zero offset, the fact that forcing the linear regressions to pass through [0,0] yields R^2 very similar to unforced regressions (also see Figure 3) means that the [WA calibration] applied gains and offsets are useful for reducing the NT ASTER mosaic to apparent reflectance. Importantly, other validation measures indicate that the associated geoscience information error is small and mostly constrained to areas of low reflectance (e.g. deep shading).

Table 1. The ASTER-Hyperion validation regression results for NT based on 117 ROIs after the WA coefficients were applied to the NT ASTER mosaic. The second columns of gains and R^2 are for a regression line that passes through 0.

band	average apparent reflectance (*10000)	gain	offset	%[offset/ average reflectance]	R^2	gain	R^2
1	1260	0.934	-50	4.0	0.79	0.89	0.79
2	1943	0.908	-25	1.3	0.81	0.896	0.81
3	2734	0.874	125	4.6	0.75	0.92	0.75
4	2800	0.817	-355	12.7	0.72	0.721	0.71
5	2409	0.823	260	10.8	0.74	0.91	0.73
6	2264	0.841	201	8.9	0.81	0.910	0.81
7	2128	0.756	294	13.8	0.79	0.860	0.78
8	2177	0.818	307	14.1	0.81	0.938	0.79
9	2252	0.923	350	15.5	0.73	1.067	0.71

Processing methodology for the ASTER's TIR bands

The pre-processing methodology for the TIR geoscience products is similar to the one implemented on the VNIR-SWIR bands, except:

- ASTER L2 emissivity data is used instead of the L1B radiance at sensor;

- Pixel size is 90 m (instead of 30 m for the VNIR-SWIR bands);
- No independent airborne/spaceborne calibration/validation data were available; and
- No masking is applied to any of the derived geoscience products.

As described above, there are no Nationally-available, independent data sets, like airborne HyMap or satellite Hyperion imagery, suitable for reduction and validation of the TIR bands though the Auscope National Virtual Core Library (NVCL – http://nvcl.csiro.au) HyLogger-3 data, which includes the TIR, could play a future role. Nevertheless, two TIR geoscience products are released here (quartz and silica indices – Table 3) and another three are currently being validated "geologically" prior to their release (Table 4). These TIR geoscience products are largely based on published work (Hewson *et al.*, 2005; Cudahy *et al.*, 2002; Ninomiya *et al.*, 2005).

Geoscience Information Extraction

There are three basic types of geoscience information products listed in Tables 2, 3 and 4, namely:

- Mineral group content;
- Mineral group composition; and
- Mineral group index.

 The rationale for these three types of geoscience products is:

- Absorption depth (relative to band/s outside of the absorption – ideally a continuum) for "content";
- Absorption geometry (wavelength) for "composition"; and
- An "index" is sensitive to the presence of material type but not specifically its content or composition.

Note that the composition and content for a given mineral group should not be correlated. By way of example, the content of AlOH group of minerals, which comprises minerals like: *muscovite, illite, phengite, kaolinite and Al-smectite*, is based on the ASTER band combination: $(B_5+B_7)/B_6$. ASTER bands 5 and 7 are located on the absorption edges and band 6 is over the 2200 AlOH absorption of these minerals. Low values represent low AlOH content and high values represent high AlOH content. Figure 5, which is based on USGS pure mineral spectra convolved to ASTER responses (http://www.ittvis.com/portals/0/tutorials/envi/Signatures_Spectral_Res.pdf), shows that this band combination separates the AlOH-bearing minerals of phengite, muscovite and kaolinite from the non-AlOH-bearing minerals, amphibole, chlorite, epidote and calcite at a threshold of 2. Without using a threshold of >2 for the AlOH abundance and applied to the B_5/B_7 ratio, then all of the non-AlOH-bearing minerals will also return an unnecessary, incorrect estimate for AlOH composition.
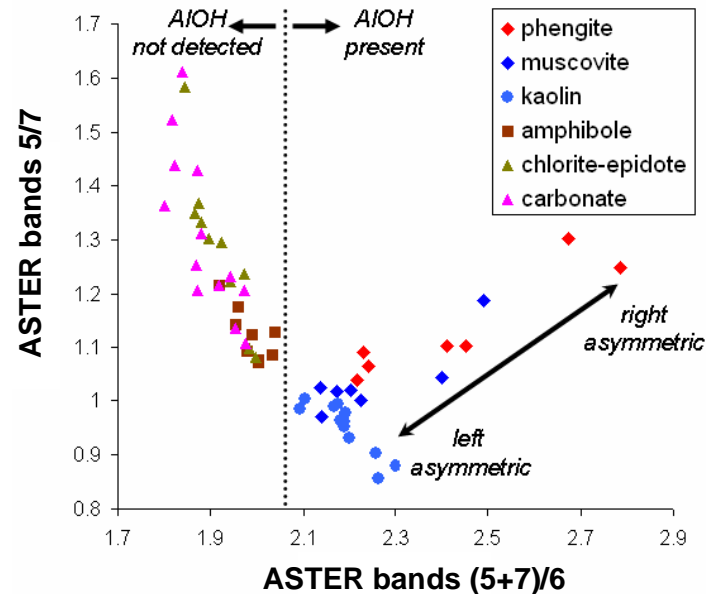
Figure 5: Scattergram of the ASTER derived "AlOH content" versus the "AlOH composition" products for a selection of pure minerals from the ENVI USGS mineral spectral library (http://speclab.cr.usgs.gov/spectral.lib06/ds231/). From Cudahy et al. (2008).

There is insufficient spectral resolution with ASTER to accurately measure the wavelength position of the Al-clay absorption minimum, which is correlated for example with Tschermak substitution in white mica (Scott and Yang, 1997). Instead, for the available ASTER bands, the relative heights of the shoulders to this 2200 nm absorption are used as a surrogate. Figure 5 shows that the phengites (Si-rich muscovite) generally produces higher B_5/B_7 values compared with the kaolins and muscovites (Al-rich). However, this compositional information becomes complicated when other materials, which also absorb at ASTER Band 5 or 7, are also involved. For example, well-ordered kaolinite and pyrophyllite can have relatively strong (to Band 6) absorption at 2160 nm (ASTER band 5) resulting in a low (even below the threshold of "2") AlOH content $[(B_5+B_7)/B_6]$ response. To help indentify this behaviour, a ratio index of B_6/B_5 is used to help map these and other 2160 nm absorbers like alunite (see Table 1 – *Kaolin Group index*).

The MgOH and carbonate content and composition products yield a similar pattern as the AlOH products (Figure 6). That is, without the applied content threshold, non-MgOH minerals like kaolin and white mica will yield similar compositional information as MgOH minerals like chlorite and amphibole and carbonate minerals like calcite and dolomite. Note also the broad compositional change from calcite to dolomite and epidote to chlorite.
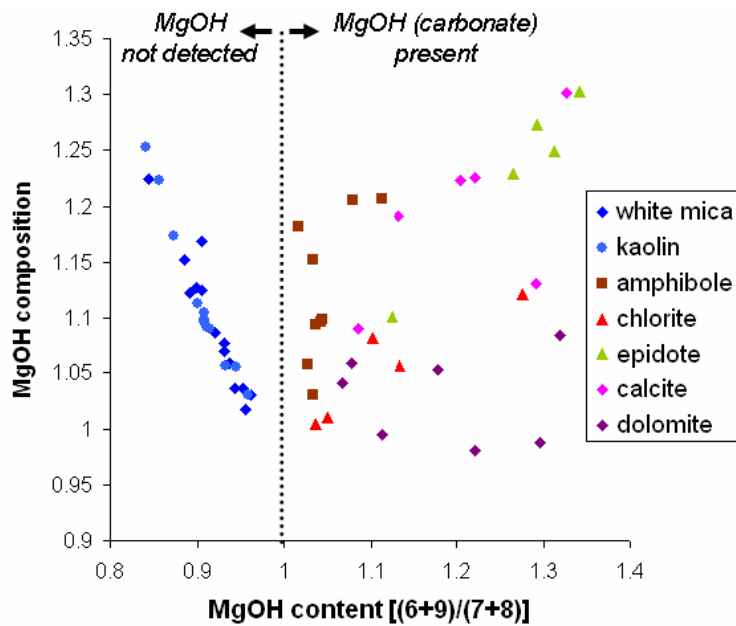
*Figure 6: Scattergram of the ASTER derived "MgOH content" versus the "MgOH composition" products for a selection of pure minerals from the ENVI USGS mineral spectral library (*From Cudahy *et al.* (2008).
(*http://speclab.cr.usgs.gov/spectral.lib06/ds231/).*

Both of the above examples show the importance of applying the associated "content" mask for the respective "composition" product. The current list of ASTER geoscience products does not involve "unmixing" to remove, for example, the effects green vegetation. It is possible to reduce the contribution of such complications using methods similar to that published by Rodger and Cudahy (2009) for the ASTER products, which could be incorporated in future ASTER product versions.

Geo-correction

The 1:1,000,000 scale NT ASTER geoscience product map-sheets are based on a GDA94 datum using a geographic latitude-longitude projection (decimal degrees). No control points were used.

ASTER SWIR sensor degradation

Later ASTER images (~2007) began to develop an instrument problem associated with decreasing dynamic range and related detector saturation for brighter pixels causing the SWIR module finally decommissioned from 2008. Evidence of this degradation is apparent in the current

mosaic for some of the 2007 scenes especially for products involving B_6 and for pixels/areas with high albedo. After normalisation, these compromised areas are effectively reduced to column striping only. Ideally these scenes should be replaced.

Geoscience Product Accuracy

Tables 2, 3 and 4 include a row called "accuracy", which is largely a qualitative estimate of accuracy (ranked as low or moderate) combined with a description of complicating factors. A number of products also include an RMSE (root mean square error) estimate based on laboratory validation studies (Haest *et al.*, 2012). These quantitative error estimates will gradually be built on as appropriate validation data is gathered. Note that these RMSE estimates are currently an under-estimation as they do not take into account the affects of mixing with green and dry vegetation in the remote sensing data. Future mineral content products that include unmixing of the vegetation component (Cudahy and Rodger, 2009) should help reduce this additional error. Ultimately, the plan is to also convert the current ratio/index values into % contents (and chemical compositions) making it easier for geoscientists, especially if the data is to be included in quantitative geological modelling.

ASTER Geoscience Products

Tables 2, 3 and 4 provide Version 1 of C3DMM's standard ASTER geoscience product list.   We recommend when importing and using the ASTER content, composition and index products in a GIS package such as ARCMAP™, to switch the null (zero) values to "see through" and then underlay each of these rainbow coloured maps with a gray-scale image, such as Band 2 of the "false colour" image.

Table 2: ASTER VNIR-SWIR Geoscience Products – Version 1.1

Product name (in red)	Base algorithm B=band No. = band No.	Masks	Stretch^ (lower limit)	Stretch^ (upper limit)	Stretch+ type
1. False colour (red = green vegetation)	Red: B3 Green: B2 Blue: B1	none	R: 361 G: 309 B: 1	R: 4241 G: 2913 B: 1961	linear
	Accuracy: n/a				
	Suggested use: Use this image to help understand non-geological differences within and between ASTER scenes caused by green vegetation (red), fire scars, thin and thick cloud and cloud shadows. Use band 2 only for a gray-scale background to the content, composition and index colour products.				
2. CSIRO Landsat TM Regoith Ratios (white = green vegetation)	R: B_3/B_2 G: B_3/B_7 B: B_4/B_7	composite mask*	R: 1.128 G: 0.697 B: 1.050	R: 1.853 G:1.530 B: 1.780	linear
	Accuracy: n/a				
	Suggested use: Use this image to help interpret (1) the amount of green vegetation cover (appears as white); (2) basic spectral separation (colour) between different regolith and geological units and regions/provinces; and (3) evidence for unmasked cloud (appears as green).				
3. Green vegetation Content	B_3/B_2	composite mask*	1.5 Blue is low content	2.5 Red is high content	linear
	Accuracy: Moderate: Complicated by iron oxides, dry vegetation and uncorrected aerosols (including smoke). Iron oxide produces a small decrease in this green vegetation product. Beware of strong seasonal variations in green vegetation content. *Note 1.* The standard NDVI [$(B_3-B_2)/(B_2+B_3)$] and the B_3/B_2 combination used are highly correlated. *Note 2.* The spectral band-passes of ASTER do not cover diagnostic dry vegetation features (e.g. cellulose at 2080 nm) such that measuring, mapping and removing the effects of dry vegetation is difficult with these data.				
	Geoscience Applications[#]: Use this image to help interpret the amount of "obscuring/complicating" green vegetation cover.				

Product name (in red)	Base algorithm B=band No. = band No.	Masks	Stretch^ (lower limit)	Stretch^ (upper limit)	Stretch+ type
4. Ferric oxide content (hematite, goethite, jarosite)	B_4/B_3	Composite mask* + green vegetation content <1.75.	1.1 Blue is low abundance	2.1 Red is high abundance	linear

Accuracy: Moderate: From laboratory validation studies of geological samples (Haest et al, 2012), the RMSE of this product is ~11%. However, this error is larger for these Version 1.1 ASTER products, given that there is no correction for mixing with green and dry vegetation.

Green vegetation is also in part, inversely proportional to this product. The applied green vegetation mask does not fully remove this green vegetation mixing affect. This produces complicating effects. Use the false colour image to help unravel this affect.

Geoscience Applications[#]:
(1) Exposed iron ore (hematite-goethite). Use in combination with the "Opaques index" to help separate/map dark (a) surface lags (e.g. maghemite gravels) which can be misidentified in visible and false colour imagery; and (b) magnetite in BIF and/or bedded iron ore; and
(2) Acid conditions: combine with FeOH Group content to help map jarosite which will have high values in both products.

Product name (in red)	Base algorithm	Masks	Stretch^ (lower limit)	Stretch^ (upper limit)	Stretch+ type
5. Ferric oxide composition (hematite, goethite)	B_2/B_1	Composite mask* + green vegetation content <1.75. + Ferric oxide content >1.3	0.5 Blue-cyan is goethite-rich Green is hematite-goethite	3.3 Red-yellow is hematite-rich	Gaussian

Accuracy: Moderate: This product is sensitive to visible colour with high values being red and low values being green/ yellow. The applied masks reduce complications caused by green vegetation and fresh "green" rocks with minerals like chlorite. However, dry vegetation can cause error. Quantitative measurement of the hematite-goethite ratio is more accurately measured using the wavelength of the 900 nm crustal field absorption (Cudahy and Ramanaidou, 1996)

Geoscience Applications[#]:
(1) Mapping transported materials (including palaeochannels) characterised by hematite (relative to goethite). Combine with AlOH composition to find areas of hematite and poorly ordered kaolin to map transported materials; and
(2) hematite-rich areas in "drier" conditions (e.g. above the water table) whereas goethite-rich in "wetter conditions (e.g. at/below the water or areas recently exposed). May also be climate-driven.

Product name (in red)	Base algorithm	Masks	Stretch^ (lower limit)	Stretch^ (upper limit)	Stretch+ type
6. Ferrous iron index (in silicates/ carbonates - actinolite, chlorite, ankerite, pyroxene, olivine, ferroan dolomite, siderite)	B_5/B_4	Composite mask* + green vegetation content <1.75.	0.75 Blue is low abundance	1.025 Red is high abundance	linear

Accuracy: Moderate: Difficult product to independently gauge accuracy as the spectrally detected ferrous iron is associated with silicate and carbonate minerals and not ferrous iron in oxides and sulphides. Issues that complicate its accuracy include: (1) ferrous iron in non-silicate/carbonate minerals, e.g. in oxides (magnetite); (2) other opaque phases such as carbon black (e.g. graphitic shales and even recent fire scars rich in black ash; (3) a lack of dry plant material, as in fire scares, which often appears as red; and (4) green vegetation which suppresses this index.

Geoscience Applications[#]: This product can help map exposed "fresh" (un-oxidised) rocks (warm colours) especially mafic rocks rich in ferrous silicates (e.g. actinolite, chlorite) and/or ferrous carbonates (e.g. ferroan dolomite, ankerite, siderite). Applying an MgOH Group content mask to this product helps to isolate ferrous bearing non-OH bearing minerals like pyroxenes (e.g. jadeite) from OH-bearing or carbonate-bearing ferrous minerals like actinolite or ankerite, respectively. Also combine with the FeOH Group content product to find evidence for ferrous-bearing chlorite (e.g. chamosite).

Product name (in red)	Base algorithm B=band No. = band No.	Masks	Stretch^ (lower limit)	Stretch^ (upper limit)	Stretch+ type
7. Opaque index (potentially includes carbon black (e.g. ash), magnetite, Mn oxides, and sulphides in "reduced" environments	B_1/B_4	Thick cloud* + sun glint* + + B4 <2500 + green vegetation <1.75	0.4 Blue is low content	0.9 Red is high content	linear
	Accuracy: Moderate**:** Complicated by "albedo" effects, cloud shadow and recent fires scars (high black ash content), smoke, other vegetation changes and any residual errors in aerosol correction. The complications with albedo arise for example with iron-oxide poor materials/pixels, such as quartz and/or clays that are equally bright at VNIR- and SWIR wavelengths. These are isolated (in part) using the albedo mask (<25%), though this can be further complicated by "shadowing" effects, e.g., clay rich pixels in shade. This product needs to be compared with the albedo and false colour infrared products to help isolate these and other complications.				
	Geoscience Applications[#]: Useful for mapping: (1) magnetite-bearing rocks (e.g. BIF); (2) maghemite gravels; (3) manganese oxides; (4) graphitic shales. *Note 1*: (1) and (4) above can be evidence for "reduced" rocks when interpreting REDOX gradients. Combine with "AlOH Group Content" (high values) and "AlOH Group Composition" (high values) products, to find evidence for any invading "oxidised" hydrothermal fluids which may have interacted with reduced rocks, i.e. site for potential new mineral (metal) precipitation.				
8. AlOH group content (phengite, muscovite, paragonite, lepidolite, illite, brammalite, montmorillonite, beidellite, kaolinite, dickite)	$(B_5+B_7)/B_6$	Composite mask* + green vegetation mask <1.75	1.95 Blue is low content	2.4 Red is high content	linear
	Accuracy: Moderate**:** From laboratory validation studies of geological samples (Haest et al, 2012), the RMSE of this product is ~5%. However, this error is larger for these Version 1.1 ASTER products, given that there is no correction for mixing with green and dry vegetation as well as any minerals with absorption at B_5 and/or B_7. These minerals include: (a) B_5 (2160 nm) absorbers like pyrophyllite, alunite and abundant well-ordered kaolinite; and (b) B_7 absorbers like chlorite/epidote, jarosite and gibbsite.				
	Geoscience Applications[#]: Useful for mapping: (1) exposed saprolite/saprock (2) clay-rich stratigraphic horizons; (3) lithology-overprinting hydrothermal phyllic (e.g. white mica) alteration; and (4) clay-rich diluents in ore systems (e.g. clay in iron ore). Also combine with AlOH composition to help map: (1) exposed in situ parent material persisting through "cover" which can be expressed as: (a) more abundant AlOH content + (b) long-wavelength (warmer colour) AlOH composition (e.g. muscovite/phengite).				

Product name (in red)	Base algorithm B=band No. = band No.	Masks	Stretch^ (lower limit)	Stretch^ (upper limit)	Stretch+ type
9. AlOH group composition	B_5/B_7	Composite mask* + green vegetation <1.75 + AlOH content $(B_5+B_7)/B_6$>1.97	0.9 Blue is well ordered kaolinite, Al-rich muscovite/ illite, paragonite, pyrophyllite, beidellite	1.3 Red is Al-poor (Si-rich) muscovite (phengite), montmorillonite	equalisation
	Accuracy: Moderate: Mixing with minerals like chlorite and carbonate and dry/green vegetation will make colours appear warmer than the actual Al-OH composition while cool colours (blue and cyan) can be compromised by mixtures with alunite and dry plant material. *Note 1*: Use in combination with the Al-OH group content to discount the geological importance of those pixels with low contents. That is, discount the value of any isolated warm-coloured pixels, such as those associated with fire scars.				
	Geoscience Applications[#]: Useful for mapping: (1) exposed saprolite/saprock can be associated with white mica or Al-smectite (warmer colours) whereas transported materials are typically associated with (poorly-ordered) kaolin-rich (cooler colours); (2) clays developed over carbonates, especially Al-smectite (montmorillonite, beidellite) will produce middle to warmers colours. (2) stratigraphic mapping based on different clay-types; and (3) lithology-overprinting hydrothermal alteration, e.g. Si-rich and K-rich phengitic mica (warmer colours). Combine with Ferrous iron in MgOH and FeOH content products to look for evidence of overlapping/juxtaposed potassic metasomatism in ferromagnesian parents rocks (e.g. Archaean greenstone associated Au mineralisation) +/- associated distal propyllitic alteration (e.g. chlorite, amphibole).				
10. Kaolin group index (pyrophyllite, alunite, well-ordered kaolinite)	B_6/B_5	Composite mask* + Green vegetation <1.4	0.925 Blue is low content	1.11 Red is high content	linear
	Accuracy: Moderate: Complicated by dry plant material, fire scars, thin cloud and AlOH poor areas dominated by "mafic" minerals.				
	Geoscience Applications[#]: Useful for mapping: (1) different clay-type stratigraphic horizons; (2) lithology-overprinting hydrothermal alteration, e.g. high sulphidation, "advanced argillic" alteration comprising pyrophyllite, alunite, kaolinite/dickite; and (3) well-ordered kaolinite (warmer colours) versus poorly-ordered kaolinite (cooler colours) which can be used for mapping *in situ* versus transported materials, respectively.				
11. FeOH group content (chlorite, epidote, jarosite, nontronite, gibbsite, gypsum, opal-chalcedony)	$(B_6+B_8)/B_7$	Composite mask* + Green vegetation <1.4	2.02 Blue is low content	2.185 Red is high content	linear
	Accuracy: Low: Complicated by cloud, especially thin cloud, as well as green and dry vegetation, carbonate (magnesite and to a lesser degree dolomite). Use in combination with the MgOH and vegetation products (including regolith ratios) to help unravel complicating vegetation effects.				
	Geoscience Applications[#]: Useful for mapping: (1) jarosite (acid conditions) – in combination with ferric oxide content (high); (2) gypsum/gibbsite – in combination with ferric oxide content (low); (3) magnesite - in combination with ferric oxide content (low) and MgOH content (moderate-high) (4) chlorite (e.g. propyllitic alteration) – in combination with Ferrous in MgOH (high); and (5) epidote (calc-silicate alteration) – in combination with Ferrous in MgOH (low).				

Product name (in red)	Base algorithm B=band No. = band No.	Masks	Stretch^ (lower limit)	Stretch^ (upper limit)	Stretch+ type
12. MgOH group content (calcite, dolomite, magnesite, chlorite, epidote, amphibole, talc, serpentine)	$(B_6+B_9)/(B_7+B_8)$	Composite mask* + green vegetation <1.4	1.01 Blue is low content	1.2 Red is high content	linear
	Accuracy: Moderate**:** Complicated by cloud, especially thin cloud, as well as dry vegetation (reddens), white mica as well as residual inaccuracies in instrument "crosstalk" correction, especially for B_9. Use in combination with the vegetation products (including regolith ratios) to help unravel complicating vegetation effects.				
	Geoscience Applications#: Useful for mapping: (1) "hydrated" ferromagnesian rocks rich in OH-bearing tri-octahedral silicates like actinolite, serpentine, chlorite and talc; (2) carbonate-rich rocks, including shelf (palaeo-reef) and valley carbonates(calcretes, dolocretes and magnecretes); and (3) lithology-overprinting hydrothermal alteration, e.g. "propyllitic alteration" comprising chlorite, amphibole and carbonate. The nature (composition) of the silicate or carbonate mineral can be further assessed using the MgOH composition product.				
13. MgOH group composition	B_7/B_8	Composite mask* + MgOH content >1.01 + green vegetation <1.4	0.6 Blue-cyan is magnesite-dolomite, amphibole, chlorite	1.2 Red is calcite, epidote, amphibole	equalisation
	Accuracy: Low**:** Complicated by cloud, especially thin cloud, as well as dry vegetation (more dry vegetation produces redder tones). Use in combination with the MgOH and vegetation products (including regolith ratios) to help unravel complicating vegetation effects.				
	Geoscience Applications#: From Figure 4, useful for mapping: (1) exposed parent material persisting through "cover"; (2) "dolomitization' alteration in carbonates – combine with Ferrous iron in MgOH product to help separate dolomite versus ankerite; (3) lithology-cutting hydrothermal (e.g. propyllitic) alteration – combine with FeOH content product and ferrous iron in Mg-OH to isolate chlorite from actinolite versus talc versus epidote; and (4) layering within mafic/ultramafic intrusives.				
14. Ferrous iron content in MgOH/ carbonate (Fe-chlorite, actinolite, siderite, ankerite) often useful for mapping mafic rocks	B_5/B_4	Composite mask* + MgOH content >1.01 + green vegetation <1.4	0.1 Blue is low ferrous iron content in carbonate and MgOH minerals like talc and tremolite.	2.0 Red is high ferrous iron content in carbonate and MgOH minerals like chlorite and actinolite.	equalisation
	Accuracy: Moderate**:** Complicated by dry and green vegetation and any inaccuracies in the MgOH content mask product (see above).				
	Geoscience Applications#: Useful for mapping: (1) un-oxidised "parent rocks" – i.e. mapping exposed parent rock materials (warm colours) in transported cover; (2) talc/tremolite (Mg-rich – cool colours) versus actinolite (Fe-rich – warm colours); (3) ferrous-bearing carbonates (warm colours) potentially associated with metasomatic "alteration"; (4) calcite/dolomite which are ferrous iron-poor (cool colours); and (5) epidote, which is ferrous iron poor (cool colours) – in combination with FeOH content product (high).				

Table 2 footnotes.

[+] All products use a rainbow colour look-up table (blue is low and red is high), except for the three band combinations, such as false colour image and Landsat TM regolith ratios which are R:G:B displays of three gray-scale input bands.

[^] The specified stretch limits are based on the cross-calibrated and reduced (using Hyperion reflectance) NT ASTER reflectance mosaic (0-10,000 range = 0-100% reflectance) and are expressed as 4*byte (floating pointing) data (in BSQ format) which were then output to 8-bit data and are also publicly available and suitable for local area re-stretching if required. Note that these stretch/threshold limits may still have some dependency on the nature of the pre-processing such that these values may need to be adjusted for processing other ASTER imagery. The stretch limits are based on optimising the information spanning the whole State. For greater contrast enhancement, the user is encouraged to obtain the associated BSQ files from the NTGS to generate local contrast stretches to suit their region of interest.

[#] Only a few geoscience uses are provided here to help show how these products can interpreted.

* Composite mask comprises:
(1) Thick cloud tops "out"; ASTER band 1 reflectance <2500 (25% reflectance);
(2) Low albedo (deep shadows and water) "out": reflectance Band 4<0.12 (12% reflectance); and
(3) Sun glint over water "out"; $(B_3-B_1)/(B_3+B_1)>0$.
Additional masks are applied for selected products, including:
(4) green vegetation "out" : ratio of bands 3/2 <1.7 or <1.4;
(5) AlOH content "in": $(B_5+B_7)/B_6 >1.97$; and
(6) MgOH content "in": $(B_6+B_9)/(B_7+B_8) > 1.01$.

Black in all products is coded as "zero" and represents either (1) below the product threshold (e.g. below a AlOH clay depth of 2); or (2) has been masked because of a complicating effect (e.g. too much green vegetation cover). It is possible to separate these two types if required though both are currently kept at zero value so that they can be set to "null data" (see through) in GIS packages.

Table 3: ASTER TIR Geoscience Products – to be released but not yet validated.

Product name (in red)	Base algorithm	Masks	Stretch (lower limit)	Stretch (upper limit)	Stretch type (for geoTIFFs)
Silica Index (Si-rich minerals, such as quartz, feldspars, Al-clays)	B_{13}/B_{10}	none	1.045 Blue is low silica content.	1.4 Red is high silica content.	linear
	Accuracy: Moderate: Strongly affected by particle size and regolith affects. For example, alluvial/colluvial materials generally show high values compared to outcrop because of the abundance of clean, coarse (>>250 micron) quartz grains. Fine particle size (<<250 micron) produces low responses. Strongly affected by cloud tops (appear as warmer colours). Affected in part by green and dry vegetation, especially fire scares. Very minor instrument related line-striping.				

	Geoscience Applications: Broadly equates to the silica content though the intensity (depth) of this reststrahlen feature is also affected by particle size <250 micron. Useful product for mapping:
	  (1) colluvial/alluvial materials;
	  (2) silica-rich (quartz) sediments (e.g. quartzites);
	  (3) silification and silcretes; and
	  (4) quartz veins.
	Use in combination with quartz index, which is often correlated with the Silica index (see below).				

Quartz Index	$B_{11}/(B_{10}+B_{12})$	none	0.506 Blue is low quartz content.	0.520 Red is high quartz content.	linear
	Accuracy: Low: Strongly affected by discontinuous line striping. Strongly affected by cloud tops (appear as warmer colours). Relatively unaffected by particle size. Best used as a discriminator of quartz rather than as a measure of quartz content.				
	Geoscience Applications: Use in combination with Silica index to more accurately map "crystalline" quartz rather than poorly ordered silica (e.g. opal), feldspars and compacted clays.				

Table 4: ASTER TIR Geoscience Products – still being validated and not yet ready for release.

Product name (in red)	Base algorithm	Masks	Stretch (lower limit)	Stretch (upper limit)	Stretch type (for geoTIFFs)
Carbonate Index (calcite, dolomite, magnesite, siderite, ankerite)	B_{13}/B_{14}	none	1.006 Blue is low carbonate content.	1.02 Red is high carbonate content.	linear
	Accuracy: Very Low: Remaining inter-scence cross-calibration errors. Strongly affected by discontinuous line striping and cloud tops (appear as warmer colours). Affected by green (blackbody) and dry vegetation. Potentially compromised by spectrally flat materials (possibly burnt areas?).				

	Geoscience Applications: Should be combined with the MgOH content to help map carbonates, that is, warm colours in both products. Alternatively, use this product to help map more confidently MgOH silicates without carbonate.				
Mafic Group Index (pyroxenes, garnets, olivine, epidote, chlorite, calcite, magnesite/dolomite) *Name change?*	B_{12}/B_{13}	none	0.96 Blue is low mafic mineral content.	1.02 Red is high mafic mineral content.	linear
	Accuracy: Low: A range of both silicate and carbonate minerals can influence this product. Strongly complicated by dry vegetation (produces warmer tones). Moderately affected by discontinuous line striping and cloud tops (appear as warmer colours). Often inversely correlated with Si-rich mineralogy/rocks. Some discontinuous line-striping.				
	Geoscience Applications: Useful for mapping: (1) carbonates, especially those richer in Mg content (e.g. magnesite and dolomite); (2) mafic rocks that comprise non-MgOH minerals, such as pyroxenes and olivines; (3) garnet and pyroxene-rich skarns; and (4) metamorphic-grade, higher temperature facies (~granulite).				
Sulphate index (alunite, talc, feldspars, AlOH group minerals) *Name change?*	B_{10}/B_{12}	none	1.01 Blue is low mafic mineral content.	1.08 Red is high mafic mineral content.	linear
	Accuracy: Very Low: Strongly complicated by dry vegetation and often inversely correlated with Si-rich mineralogy/rocks. Affected by discontinuous line-striping.				
	Geoscience Applications: Useful for mapping: (1) feldspar-bearing granite and rhyolite; (2) talc alteration;				

Data Access

- The NT wide ASTER ecw images are availalable through the NTGS Geophysical Image Web Server (http://geoscience.nt.gov.au/giws/)
- The NT ASTER geoscience 1M map sheets (each map sheet is ~100 Mbytes) are provided as GIS-compatible geoTIF formats and obtainable from:
    - CSIRO C3DMM's portal for ftp download (http://c3dmm.csiro.au); and
    - Auscope Grid portal (http://portal.auscope.org/portal/gmap.html) under "Registered Layers";
- The related raster files of these products in BSQ (Band Sequential) and BIL (Band Interleaved Line) format (~500 Gigabytes) and either

ERMapper or ENVI Headers can only be obtained from NTGS InfoCentre (http://infocentre.altarama.com/reft100.aspx?key=REQU) via an external hard drive; and

- The NT ASTER reflectance mosaic, also in BSQ/BIL format, is only accessible to CSIRO and the government geosurveys as part of a copyright agreement with ERSDAC (Japan).

Future Work

A summary of the next steps leading to release of the Australian ASTER geoscience map Version 1 in August 2012 at the 34IGC are as follows:

- Vegetation unmixing developed and tested – potential for release as part of later product Version number (post August 2012). This includes assessment of whether dry vegetation content can be estimated with sufficient accuracy from the available ASTER bands spectral resolution;
- Linking of an "ASTER-convolved" NVCL library to the public ASTER geoscience map through for example the Auscope grid portal (http://www.auscope.org.au/site/grid.php);
- Quantifying product accuracies (ongoing);
- Journal publications on the processing methodology and geological case histories prepared and submitted; and
- Linking/extending this National ASTER geoscience initiative to global geoscience mapping programs (e.g. GEOSS - http://www.earthobservations.org/geoss.shtml).

Acknowledgements

C3DMM's development portal though this function has now being transitioned to CSIRO's IMT facilities. Useful editorial comments to the draft document were provided by Mike Caccetta, Simon Collings and Carsten Laukamp from CSIRO. To all of these people and organisations we express our sincere thanks.

References

- Abrams, M., Hook, S and Ramachandran, B., 2002. ASTER user handbook. JPL Publication 2, 135 pp.
- Cudahy, T.J. and Ramanaidou, E.R.., 1996. Measurement of the hematite-goethite ratio using field VNIR spectrometry in channel iron deposits, Western Australia. *Australian Journal of Earth Sciences*, Vol. 44, No. 4, pp. 411-421.
- Cudahy, T.J., Okada, K., Cornelius, A., and Hewson, R.D. (2002). Regional to prospect scale exploration for porphyry-skarn-epithermal mineralisation at Yerington, Nevada, using ASTER and airborne Hyperspectral data. CSIRO Exploration and Mining Report, 1122R, 26 pages (ftp://ftp.arrc.csiro.au/NGMM/Thermal_Reports).
- Cudahy T.J., Caccetta, M., Cornelius, A., Hewson, R.D., Wells, M., Skwarnecki, M., Halley, S., Hausknecht, P., Mason, P. and Quigley, M.A., 2005. Regolith geology and alteration mineral maps from new generation airborne and satellite remote sensing technologies and Explanatory Notes for the Kalgoorlie-Kanowna 1:100,000 scale map sheet, remote sensing mineral maps. MERIWA Report No. 252, 114 pages (http://c3dmm.csiro.au/kalgoorlie/kalgoorlie.html).
- Cudahy, T.J., Jones, M., Thomas, M., Laukamp, C., Caccetta, M., Hewson, R.D., Rodger, A.D. and Verrall, M., 2008. Next Generation Mineral Mapping: Queensland Airborne HyMap and Satellite ASTER Surveys 2006-2008. CSIRO report P2007/364, 153 pages (http://c3dmm.csiro.au/NGMM/index.html)
- Haest, M., Cudahy, T.J. and Laukamp, C., 2012. Quantitative mineralogy from infrared spectroscopic data: I. Validation of mineral abundance and composition scripts at the Rocklea channel iron deposit in Western Australia. *Economic Geology* (in press).
- Hewson, R.D., Cudahy, T.J., Mizuhiko S., Ueda, K., Mauger, A.J., 2005. Seamless geological map generation using ASTER in the Broken Hill-Curnamona province of Australia. *Remote Sensing of Environment*, 99, pp. 159–172.
- Hewson, R.D., and Cudahy, T.J., 2010. Issues affecting geological mapping with ASTER data: A case study of the Mount Fitton area, South Australia.' Chapter 13. In *Land Remote Sensing and Global Environmental Change: NASA's Earth Observing System and the Science of ASTER and MODIS.* Eds. Ramachandran, B, Justice, C, and Abrams M., Springer, New York, *273-300.*
- Hulley, G.C. and Hook, S.J, 2009. The North American ASTER Land Surface Emissivity Database (NAALSED) Version 2.0. *Remote Sensing of Environment*, 113, 1967–1975.

- Iwasaki, A. and Tonooka, H., 2005. Validation of a Crosstalk Correction Algorithm for ASTER/SWIR. *IEEE Transactions on Geoscience and Remote Sensing,* Vol. 43, No. 12, pp. 2747-2751.
- NASA's Earth Observing System, 2011. Land remote sensing and global environmental change. NASA's Earth Observing System and the Science of ASTER and MODIS. Eds. Ramachandran, B., Justice, C.O., and Abrams, M.J., Remote Sensing and Digital Image Processing, Volume 11, Springer, 873 pages.
- Ninomiya, Y., Fu, B., and Cudahy, T. J., 2005. Detecting lithology with Advanced Spaceborne Thermal Emission and Reflection Radiometer (ASTER) multispectral thermal infrared "radiance-at-sensor" data. *Remote Sensing of Environment*, 99, pp. 127-139.
- Oliver, S. and van der Wielen, S., 2005. Mineral mapping with ASTER. *AusGeo News*, Geoscience Australia, Issue 82, June 2005, (http://www.ga.gov.au/image_cache/GA8238.pdf).
- Rodger, A. & Cudahy, T. (2009): Vegetation corrected continuum depths at 2.20µm: An approach for hyperspectral sensors. - *Remote Sensing of Environment*, 113, 2243-2257.
- Rowan, L.C., Hook, S.J., Abrams, M.J. and Mars, J.C., 2003. Mapping hydrothermally altered rocks at Cuprite, Nevada, using the Advanced Spaceborne Thermal Emission and Reflection Radiometer (ASTER), a new satellite-imaging system. *Economic Geology*, 98:1019–1027.
- Rowan, L.C. and Mars J.C., 2003. Lithologic mapping in the Mountain Pass, California area using Advanced Spaceborne Thermal Emission and Reflection Radiometer (ASTER) data. *Remote Sensing of Environment,* 84:350–366.
- Scott, K. and Yang, K., 1997. Spectral Reflectance Studies of white micas. CSIRO Exploration and Mining Report No. 439R, 41pp.

Contacts

Geoscience applications and data processing
Dr Thomas Cudahy
Director, Western Australian Centre of Excellence for 3D Mineral Mapping (C3DMM)
CSIRO Earth Science and Resource Engineering
Australian Resources Research Centre (ARRC)
Street: 26 Dick Perry Avenue, Kensington, WA. Australia, 6151
Postal: PO Box 1130, Bentley. WA, Australia, 6102
phone: 618-6436-8630 ; mobile: 61-407-662-369 ; fax: 618-6436-8586
email: thomas.cudahy@csiro.au

CSIRO/Auscope ASTER web delivery
Peter Warren
CSIRO Earth Science and Resource Engineering
Riverside Life Sciences Centre, 11 Julius Avenue,
Northe Ryde, N.S.W., 2113.
phone: 612- 9490 8802 ; fax : 612-9490 8921
email: peter.warren @csiro.au